

General Disclaimer

One or more of the Following Statements may affect this Document

- This document has been reproduced from the best copy furnished by the organizational source. It is being released in the interest of making available as much information as possible.
- This document may contain data, which exceeds the sheet parameters. It was furnished in this condition by the organizational source and is the best copy available.
- This document may contain tone-on-tone or color graphs, charts and/or pictures, which have been reproduced in black and white.
- This document is paginated as submitted by the original source.
- Portions of this document are not fully legible due to the historical nature of some of the material. However, it is the best reproduction available from the original submission.

Radiographic Detectability Limits for Seeded Voids in Sintered Silicon Carbide and Silicon Nitride

(NASA-TM-86945) RADIOGRAPHIC DETECTABILITY LIMITS FOR SEEDED VOIDS IN SINTERED SILICON CARBIDE AND SILICON NITRIDE (NASA) 19 p
HC A02/MF A01 CSCL 14D N85-21674
G3/38 Unclass 14612

George Y. Baaklini, James D. Kiser,
and Don J. Roth
*Lewis Research Center
Cleveland, Ohio*

Prepared for
The Regional Meeting of the American Ceramic Society
San Francisco, California, October 28-31, 1984

NASA



**RADIOGRAPHIC DETECTABILITY LIMITS FOR SEEDED VOIDS IN SINTERED
SILICON CARBIDE AND SILICON NITRIDE**

George Y. Baaklini, James D. Kiser, and Don J. Roth
National Aeronautics and Space Administration
Lewis Research Center
Cleveland, Ohio 44135

SUMMARY

Conventional and microfocus x-radiographic techniques were compared to determine relative detectability limits for voids in green and sintered SiC and Si₃N₄. The relative sensitivity of the techniques was evaluated by comparing their ability to detect voids that were artificially introduced by a seeding process. For projection microfocus radiography the sensitivity of void detection at a 90/95 probability of detection/confidence level is 1.5 percent of specimen thickness in sintered SiC and Si₃N₄. For conventional contact radiography the sensitivity is 2.5 percent of specimen thickness. It appears that microfocus projection radiography is preferable to conventional contact radiography in cases where increased sensitivity is required and where the additional complexity of the technique can be tolerated.

INTRODUCTION

The strength-limiting defects commonly observed in sintered silicon-base ceramics such as SiC and Si₃N₄ include pores, microcracks, inclusions, and variations in the microstructure (refs. 1 to 3). During the fabrication process inclusions are introduced, and pores and microcracks are formed. X radiography can be used as a nondestructive evaluation tool to detect and identify these flaws. However, the limits of x-ray detectability of defects have to be evaluated and proven applicable to defects that are fracture causing and strength limiting (critical size defects) in sintered structural ceramics.

Conventional and microfocus x radiography have been used to evaluate structural ceramics. Kossowsky (ref. 4) and Richerson et al. (ref. 5) have reported limits of resolution for defects in hot-pressed and reaction-bonded Si₃N₄. The sensitivity capabilities reported were on the order of 0.5 percent of thickness for high density inclusions and on the order of 3 percent of thickness for clusters of voids. The ability to detect voids in structural ceramics is vital for better and more reliable ceramics. Further evaluation of the sensitivity of radiographic techniques and the establishment of reliability statistics for void detection are needed.

The purpose of this paper is to compare the reliability of two different x-radiographic techniques in finding seeded single voids in green and sintered SiC and Si₃N₄. For the void/ceramic system the contrast is generally poor when using conventional radiography with relatively high x-ray photon energy (58 to 70 keV). It will be shown that radiographic detectability of the void-ceramic system is substantially enhanced when using low x-ray photon energy (17 to 20 keV) in a microfocus system operating in the projection mode. In addition, detection probability statistics are established for a representative range of (artificially seeded) voids.

THEORY AND DATA ANALYSIS

Radiographic detectability depends on the spatial resolution of the radiographic system and on the image contrast recorded by the radiographic detector. The spatial resolution is a function of the film (detector) graininess, which governs signal-to-noise ratio, and the geometric unsharpness U_g , given by

$$U_g = f \frac{b}{a} \quad (1)$$

where f is the focal spot size, a is the source-to-object distance, and b is the object-to-film distance. Resolution is improved by using fine-grained film and an experimental setup with small geometric unsharpness values (smaller than the defect under evaluation). In conventional contact radiography, the geometric unsharpness is limited by the focal spot size, f , which is typically equal to or greater than $400 \mu\text{m}$. In projection microfocus radiography, it is limited by the ratio b/a . To maximize detectability, it is necessary to have a spatial resolution smaller than the defect size under evaluation and a high image contrast to record the differences in x-ray absorption between the defect and the matrix. The image contrast (ref. 6) is given by

$$\text{Contrast} = \frac{0.43(\mu_1 - \mu_2)DG_r}{1 + I_s/I_d} \quad (2)$$

where μ_1 is the attenuation coefficient of the matrix, μ_2 is the attenuation coefficient of the defect, D is the thickness of the defect in the direction of the x-ray beam, G_r is the film gradient, I_s is the intensity of the scattered radiation, and I_d is the intensity of the direct image-forming radiation. As shown by equation (2), a smaller ratio I_s/I_d and a larger difference $\Delta\mu = \mu_1 - \mu_2$ are needed to improve the image contrast. In projection radiography the ratio I_s/I_d is smaller than in conventional radiography, which improves the image contrast (ref. 7). The difference in x-ray absorption between the defect and the matrix increases when x-ray photon energy decreases (ref. 8). However, for voids in SiC and Si₃N₄ the differential in absorption even at low x-ray photon energies is too small to enhance the image contrast. Nevertheless, image contrast can be increased by the use of a low x-ray photon energy system in the projection mode and by optimizing exposure conditions.

Radiographic detectability of defects expressed as a percent of thickness sensitivity is given by

$$\text{Thickness sensitivity} = \frac{D}{T} 100 \quad (3)$$

where D is the dimension of the defect in the x-ray beam direction and T is the thickness of the matrix specimen in the same direction.

The examination of the seeded specimens was based on either detecting or not detecting existing voids. Since only two outcomes from this examination are possible, it can be described by a binomial distribution. Detection is probabilistic in nature due to the inspection uncertainty associated with equipment, operator performance, shape and orientation of flaws, etc. The degree of confidence in the probability of detection is limited by the number

of seeded flaws. The statistical treatment used to determine the reliability of the techniques is given by the expression (ref. 9):

$$1 - G = \sum_{X=S}^N \frac{N!}{X!(N-X)!} P_L^X (1 - P_L)^{N-X} \quad (4)$$

where P_L is the lower-bound probability of detection, G is the confidence level, N is the total number of flaws, and S is the number of detected flaws. The optimized-probability method (ref. 9) was used to subdivide the thickness sensitivity data into small intervals and to plot reliability curves for each of the techniques and materials under consideration. This method was chosen because the thickness sensitivity (void size) data were not uniformly distributed throughout the data range and the number of voids in specific intervals was limited.

SPECIMEN PREPARATION AND CHARACTERIZATION

General Approach

The SiC and Si₃N₄ test bars containing seeded voids, that is, cavity-type defects, were prepared and examined. Surface and internal voids were created by seeding the test bars (3.7 by 0.7 by 0.2 to 0.5 cm) with styrene divinyl benzene microspheres which were subsequently decomposed. All specimens were prepared and examined in the green state first and were examined again after sintering.

Green Specimens with Surface Voids

Selected amounts of -100 mesh α -SiC powder or -100 mesh Si₃N₄ powder containing yttria and silica sintering additives were pressed at 60 MPa in a double-action tungsten-carbide-lined die. The resultant test bar was left in the die, and the surface of the bar was dusted using a moisture-free aeroduster in order to remove loose powder. Styrene divinyl benzene microspheres with three specific diameters: 115, 80, or 50 μ m, were placed on the surface of the test bar and manipulated until approximately 20 microspheres were positioned along the longitudinal axis of the specimen. Next, the spheres were pressed into the surface of the test bar at a pressure of 120 MPa. The specimen was removed from the die, and its surfaces were dusted. Final compaction of the green specimen was accomplished by vacuum sealing the seeded test bar in thin-wall latex tubing and cold isopressing the sample at 420 MPa. The seeded specimens were then heated under vacuum to 525 °C (45-min hold at maximum temperature) to decompose the styrene divinyl benzene spheres. Once again, the surface of each specimen was dusted to remove any debris from the intentionally created surface voids. Finally, the dimensions of the samples were measured, and their densities were calculated. The surface voids, which resembled craters, were fully characterized (see table I) using a metallograph. Void positions were photographically recorded.

Green Specimens with Internal Voids

The method used to create internal voids in SiC and Si₃N₄ test bars was similar to the technique used to create surface voids. The initial forming procedure, using microspheres with diameters of 115, 80, and 50 μm was unchanged. However, a slightly lower pressure (90 MPa) was used to press the microspheres into the test bar. Next, the positions of the spheres (later voids) were photographically recorded. Then, more powder was placed in the die and compacted at 120 MPa in order to form a specimen containing seeded internal defects at known positions. The final green densification and sphere decomposition heat treatment were the same as for surface voids. The dimensions of the resultant internal voids were inferred by the destructive examination of other similarly seeded specimens.

Sintering Seeded Specimens

All Si₃N₄ test bar samples were sintered at 2140 °C for 2 hr under a static nitrogen pressure of 5 MPa. The SiC specimens were sintered at 2200 °C for 30 min under an argon pressure of 0.1 MPa. Sintered test bars with seeded voids were characterized in the same manner as the green test specimens (see table I).

Seeded Void Morphology

During the decomposition of the microsphere seeds, some of the powder which had been in contact with the microspheres was drawn into the resulting cavities. This powder was removed from the craters (seeded surface voids) by dusting the surface of the specimens. Typical surface void morphologies in the green and sintered states are shown in figure 1. It was impossible to eliminate the powder from the internal voids (fig. 2). During sintering, the powder densified and formed clusters of grains within the shrinking cavities (figs. 2(c) and (d)). These cavities resemble naturally occurring internal voids.

Specimen Characteristics

The physical characteristics of the seeded bars are presented in table I. The seeded test bars that were prepared for this study had the same densities and compositions as typical green and sintered Si₃N₄ and SiC. Surface voids were nearly hemispherical or semielliptical in the SiC and Si₃N₄ specimens except in two cases. First, for green Si₃N₄ bars seeded with 115 μm spheres, the depth of the craters was 40 percent greater than half the diameter of the opening. This was probably due to the application of an excessive pressure during the die pressing operation. Second, for sintered Si₃N₄ bars seeded with 80 and 115 μm spheres, the depth of the craters was 50 to 70 percent greater than half the diameter of the opening. Although the precise mechanism governing the cavity shape after sintering is unclear, it was probably affected by green density variations in the immediate vicinity of the cavity.

RADIOGRAPHIC TECHNIQUES

Two film radiographic techniques, one with a conventional x-ray source using the contact method and one with a microfocus source using the projection method, were compared (see fig. 3).

The conventional x-ray system with a tungsten target and a 400- μm focal spot was operated in the 25- to 75-kV range with a beam current range of 5 to 8 mA. Test bars were positioned 92 cm away from the source of radiation and in direct contact with the x-ray film. The exposure varied from 5 to 12 min, depending on other exposure parameters, in order to produce an acceptable film density range of 1.5 to 2.5.

The microfocus x-ray system with a molybdenum target and a 10- μm focal spot was operated in the 30- to 60-kV range with a beam current range of 0.25 to 0.32 mA. Test bars were positioned between the source and the film detector in order to produce an x-ray image with a magnification of approximately $\times 2.5$ and with overall source-to-film distance equal to 30 cm. The exposure varied from 10 to 20 min.

All radiographs were manually developed. To obtain uniform results, extra care was taken to eliminate film artifacts, maintain chemical concentrations, control solution temperatures and processing times, and prevent overexposure or underexposure by densitometric control. Radiographs were examined with the aid of a $\times 7$ measuring magnifier under variable intensity backlighting (1000 to 9000 lm/m^2) and in subdued room lighting.

RESULTS AND DISCUSSION

Specimen Selection

The ceramic specimen preparation technique was successful in creating seeded test bars with properties that were identical to those of typical SiC and Si_3N_4 materials (i.e., same density, composition, surface roughness, etc.). The seeding process did not introduce any other undesirable defects.

As shown in table I, the coefficient of variance data for the void depths and void diameters demonstrated that the seeding process reliably produced uniformly sized surface voids. However, more work is still needed in order to understand the effect of sintering conditions on the material surrounding the craters in the Si_3N_4 specimens. Further studies should attempt to optimize the forming of hemispherical craters.

The seeded internal voids (figs. 2(c) and (d)) were identical to typical naturally occurring voids. But, because it was difficult to fully characterize these seeded internal voids, they were considered to be inappropriate for establishing reliability statistics. Hence, only the specimens containing fully characterized surface voids (see table I) were used to study the reliability of void detection for the two techniques used.

Reliability of Void Detection

Figures 4 and 5 show the distribution of flaws (seeded/detected) over the thickness sensitivity range in green and sintered materials. Because (1) the thickness sensitivity data were not uniformly distributed throughout the data range and (2) the number of voids in specific intervals was limited, the optimized-probability method (r. f. 9) was used to subdivide the thickness sensitivity data into small intervals and to plot reliability curves for each of the techniques and materials under consideration (figs. 5 and 7). It should be noted that the plotted values of the probability of detection P_L are conservative because they are biased toward smaller, harder-to-detect voids. In other words, each point on the curve corresponds to the largest flaw size contained in the interval for which it was calculated. The horizontal bars indicate the size range over which each P_L was calculated. All reliability curves were generated at a confidence level of 95 percent.

Green silicon nitride. - The 280 surface voids in the green Si_3N_4 specimens were fully characterized metallographically and examined radiographically. The corresponding reliability curves, obtained using the optimized-probability method, are shown in figure 5(a). The thickness sensitivity at the 90/95 POD/CL (probability of detection/confidence level) was about 1.7 percent for microfocus and about 3.8 for conventional radiography. Thus, at these thickness sensitivities, there is a 95 percent confidence that the true probability of detection is greater than 90 percent (or conversely a 5 percent chance that the true POD is less than 90 percent).

Sintered silicon nitride. - The 280 surface voids in the sintered Si_3N_4 specimens were fully characterized metallographically and examined radiographically. Thickness sensitivity improved following sintering for both microfocus and conventional radiography (fig. 5(b)), being about 1.5 percent for microfocus and about 2.5 percent for conventional radiography at the 90/95 POD/CL. This improvement in detection was due to the greater difference in x-ray absorption between the sintered ceramic matrix and the craters (seeded surface voids). The matrix increased in density from less than 60 percent of theoretical in the green state to near full theoretical in the sintered state.

Green silicon carbide. - In the case of green SiC specimens 250 surface voids were characterized and examined radiographically. The radiographic sensitivity was 1.4 percent of thickness for microfocus at 90/95 POD/CL (fig. 7(a)). Microfocus was more sensitive to the presence of voids in green SiC than in green Si_3N_4 because the green density of SiC specimens was 13 percent greater than the green density of the Si_3N_4 specimens and because in general silicon carbide attenuates x rays more than silicon nitride does. The reliability curve obtained for conventional radiography (see fig. 7(a)) shows that the probability of detection is less than 80 percent in the range of 1.5 to 2.1 percent thickness sensitivity. But this is better than the POD for green Si_3N_4 (see fig. 5(a)) in the same size range. Larger voids were not available to determine the thickness sensitivity at the 90/95 POD/CL.

Sintered silicon carbide. - The seeded SiC bars were sintered and 200 surface voids were inspected. Figure 7(b) shows only the reliability of void detection curve for projection microfocus radiography. With conventional radiography, the radiographic contrast was poor, and it was difficult to discern seeded voids from naturally occurring ones. Thus, a reliability curve was not obtained for conventional radiography. A comparison of figure 8(a) with

figures 8(b) and (c) shows (1) that microfocus radiography has detected not only all of the seeded surface voids shown in figure 8(a) (void sizes ranged from 1.7 to 1.9 percent of the sample thickness), but also many naturally occurring voids (light spots) and (2) that no seeded surface voids could be discerned using conventional radiography. At 90/95 POD/CL the thickness sensitivity for microfocus radiography was about 1.5 percent. This was slightly lower than the 1.4 percent thickness sensitivity observed in green SiC. The lower sensitivity level can be attributed to the confusion of seeded voids with additional voids formed during sintering (sintered density, 97 percent of theoretical).

Internal voids. - An investigation of the microfocus radiographic detectability of internal voids was also performed. Qualitative results are shown in table II. The dimension of the resulting seeded cavity (within the green ceramic) along the x-ray path was about 20 percent smaller than the original diameter of the seeded microsphere, because the cavity was partially filled with powder following microsphere decomposition. After sintering the volume of the resulting cavity was reduced to about 35 to 40 percent of the original volume of the seeded microsphere due to (1) overall shrinkage of the cavity and (2) the presence of clusters of grains projecting from the original cavity walls. As shown in table II the detectability of internal voids made using 115- μm spheres (representing a thickness sensitivity of ≥ 1.7 percent) was excellent. However, the detectability of the voids made using 80- and 50- μm spheres (representing a thickness sensitivity of ≤ 1.3 percent) was poor. The differential in absorption for the internal-void/ceramic-matrix system is similar to the one for the surface-void/ceramic-matrix system. Hence, the results shown in table II were expected based on the comparison of the thickness sensitivities of the internal voids and surface voids at 90/95 POD/CL using microfocus x-radiography.

An unexpected result was the radiographic appearance of the internal voids in sintered silicon nitride. These voids appeared as regions of higher density than the surrounding matrix (light spots on the radiograph). It is assumed this phenomenon occurred because the material directly surrounding the cavity densified more than the matrix and/or because this material has a different chemical composition than the matrix and thus has enhanced radiographic attenuation. In either case this made the internal voids (fabricated using 80 μm spheres) easier to detect as indicated in table II.

CLOSING REMARKS

The dimensions of the seeded voids in this study were selected to span a range of sizes considered critical in sintered structural ceramics. A key factor in our approach was to have unambiguous foreknowledge of the actual size and location of each void. This was essential to establish probability-of-detection statistics in the silicon carbide and silicon nitride test bars and to render an accurate, quantitative comparison of the relative sensitivities of the two x-ray techniques studied.

Thickness sensitivity rather than specific void diameter was selected as the basis of the probability-of-detection statistics for two reasons: (1) void detectability depends primarily on image contrast sensitivity and secondarily on image spatial resolution; and (2) void detectability is a function of variations in the material thickness. In the test samples studied and in potential

ceramic components, these thickness variations can significantly affect image contrast for a given flaw size. In addition, bulk density variations introduced during specimen processing will affect the image contrast of voids. Density variations within the test bars undoubtedly influenced the detectability of individual voids and, hence, the probability-of-detection statistics presented herein.

This study demonstrated that microfocus projection radiography enhanced void detectability over conventional contact radiography. Thickness sensitivity improved by 2 percent in the green material and by 1 percent in the sintered material. This improvement was attributed to several factors: (1) smaller focal spot size; (2) projection method; (3) target material; and (4) softer radiation. However, soft x rays would preclude examination of thick samples and would extend the exposure time needed to form the radiographic image. Further, in the projection mode the area available for specimen examination is reduced. Therefore, more effort and time are needed to evaluate ceramic specimens using microfocus radiography than contact conventional radiography with its relatively hard x rays.

The results suggest the use of void detection in green structural ceramic materials to help eliminate extra operational costs by rejecting unsuitable green parts. Furthermore, ceramic specimens of the green and sintered material with seeded voids, similar to the ones developed in this research, can be used as standards to evaluate the image quality of subsequent radiographs.

CONCLUSION

The reliability of projection microfocus and direct contact conventional x-radiographic techniques in finding seeded, single voids in green and sintered SiC and Si₃N₄ were compared. This work has shown that microfocus x-radiography substantially increased the void detection capability. In the green state an improvement in thickness sensitivity of 2 percent was obtained at the 90/95 probability of detection/confidence level. In the sintered material an improvement in thickness sensitivity of 1 percent was obtained at 90/95. Although projection microfocus radiography entails more time and effort than conventional radiography, it merits use where the additional sensitivity is mandatory.

REFERENCES

1. A.G. Evans, G.S. Kino, B.T. Khuri-Yakub, and B.R. Tittman, "Failure Prediction in Structural Ceramics," Mater. Eval., **35** [4] 85-96 (1977).
2. R.W. Rice, J.J. Mecholsky, S.W. Frieman, and S.M. Morey, "Failure Causing Defects in Ceramics: What NDE Should Find," NRL-MR-4075, Naval Research Laboratory, October 30, 1979. (AD-A078234.)
3. A.G. Evans, "Structural Reliability: A Processing-Dependent Phenomenon," J. Am. Ceram. Soc., **65** [3] 127-137 (1982).
4. R. Kossowsky, "Defect Detection in Hot-Pressed Silicon Nitride," pp. 665-685, in Ceramics for High Performance Applications, edited by J.J. Burke, A.E. Gorum, and R.N. Katz, Brook Hill Publishing Co., Chestnut Hill, MA, 1974.

5. D.W. Richerson and K.M. Johansen, "Ceramic Gas Turbine Engine Demonstration Program," REPT-21-4410, Garret Turbine Engine Co., Phoenix, AZ, May 1982. (AD-A117088.)
6. R.W. Parish, "High Resolution in the Aero-Engine Industry," in Non-Destructive Inspection Methods for Propulsion Systems and Components, AGARD-LS-103, Advisory Group for Aerospace Research and Development, Nevilly-Sur-Seine, France, 1979. (AD-A069901.)
7. R.L. Smith, "The Effect of Scattering on Contrast in Microfocus Projection X-Radiography," Br. J. Non-Destr. Test., 22 [5] 236-239 (1980).
8. "Radiological Health Handbook," U.S. Department of Health, Education, and Welfare, pp. 137-140, January 1970.
9. P.F. Packman, S.J. Klima, R.L. Davies, J. Malpani, J. Moyzis, W. Walker, B.G.W. Yee, and D.P. Johnson, "Reliability of Flaw Detection by Nondestructive Inspection," pp. 414-424, in Metals Handbook, Vol. 11, 8th ed. Edited by H.E. Boyer, American Society for Metals, Metals Park, OH, 1976.

TABLE I. - SURFACE VOIDS/TEST BARS CHARACTERISTICS

Material	State	Specimen thickness range, mm	Specimen density, g/cc		Sphere size, μm	Number of voids	Void depth, μm			Void diameter, ^a μm		
			Mean	Standard deviation			Mean	Standard deviation	COV, ^b percent	Mean	Standard deviation	COV, percent
Si ₃ N ₄	Green	2.610 - 5.080	1.867	0.010	50	75	32	2	6.25	55	4	7.27
					80	73	53	3	5.66	89	6	6.74
					115	75	83	5	6.02	117	5	4.27
	Sintered	2.140 - 4.140	3.230	0.008	50	46	32	4	12.50	57	4	7.01
					80	72	66	8	12.12	85	4	4.70
					115	75	95	10	10.53	112	5	4.46
SiC	Green	3.350 - 4.550	2.111	0.028	50	25	25	2	6.00	59	5	8.47
					80	24	39	6	15.38	104	8	7.60
					115	150	58	4	6.90	142	9	6.34
	Sintered	2.900 - 3.930	3.126	0.026	50	23	22	3	13.63	50	7	14.00
					80	17	36	4	11.11	93	9	9.68
					115	150	55	5	9.09	124	8	6.45

^aVoid diameter is the crater opening diameter (perpendicular to the x-ray beam direction).

^bCOV denotes coefficient of variance, equal to (standard deviation/mean) x 100.

^cAs reported by the manufacturer standard deviation = 3.1 μm and COV = 6.2 percent.

^dAs reported by the manufacturer standard deviation = 5.2 μm and COV = 6.5 percent.

^eAs reported by the manufacturer standard deviation = 6.3 μm and COV = 5.5 percent.

TABLE II. - DETECTABILITY OF INTERNAL VOIDS USING MICROFOCUS RADIOGRAPHY

Sphere size, μm	SiC		Si ₃ N ₄	
	Green	Sintered	Green	Sintered
	Average thickness, mm			
	4.36	3.77	4.85	4.02
115	Excellent ^a	Excellent ^a	Excellent ^a	Excellent ^c
80	Poor ^b	Poor ^b	Poor ^b	Excellent ^d
50	None	None	None	None

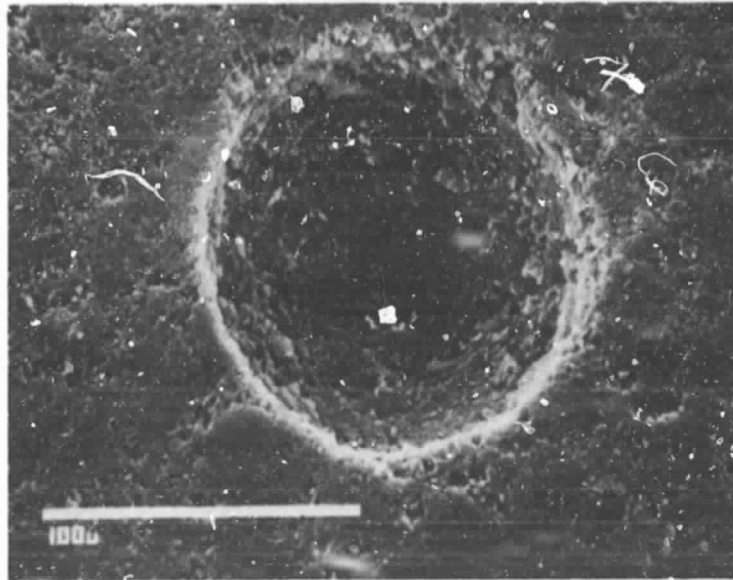
^aExcellent indicates that all seeded voids were detected.

^bPoor indicates that fewer than 50 percent of the seeded voids were detected.

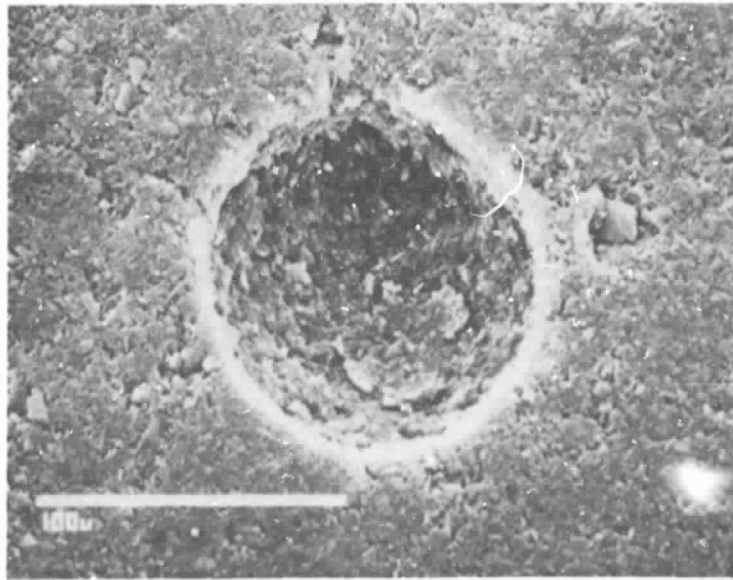
^cAll voids detected appeared as high density indications on the radiograph.

^dAll voids detected appeared as high density indications on the radiograph (with poor radiographic contrast compared with the larger voids).

ORIGINAL PAGE IS
OF POOR QUALITY



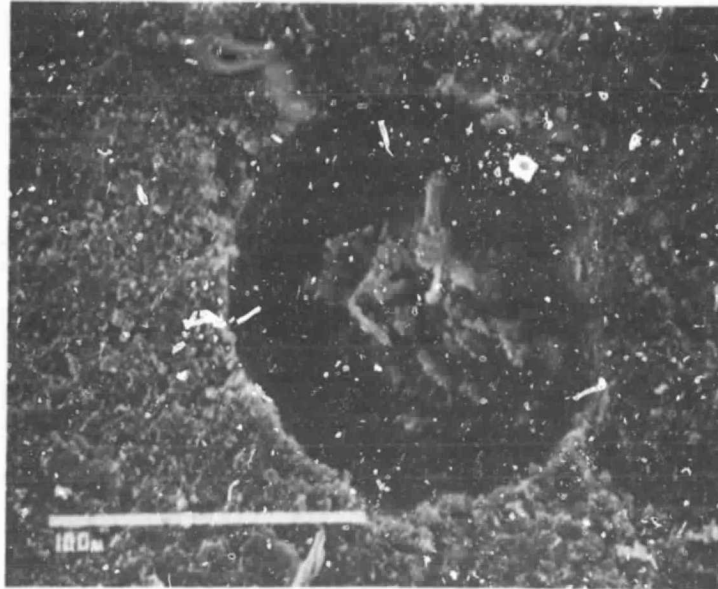
(a) Green isopressed SiC.



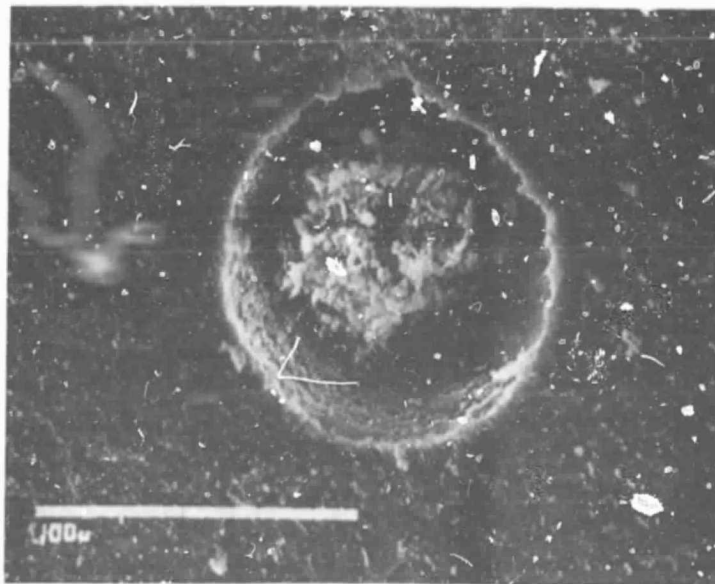
(b) Sintered SiC.

Figure 1. - Scanning electron micrographs of surface voids in SiC bars.

ORIGINAL PAGE IS
OF POOR QUALITY



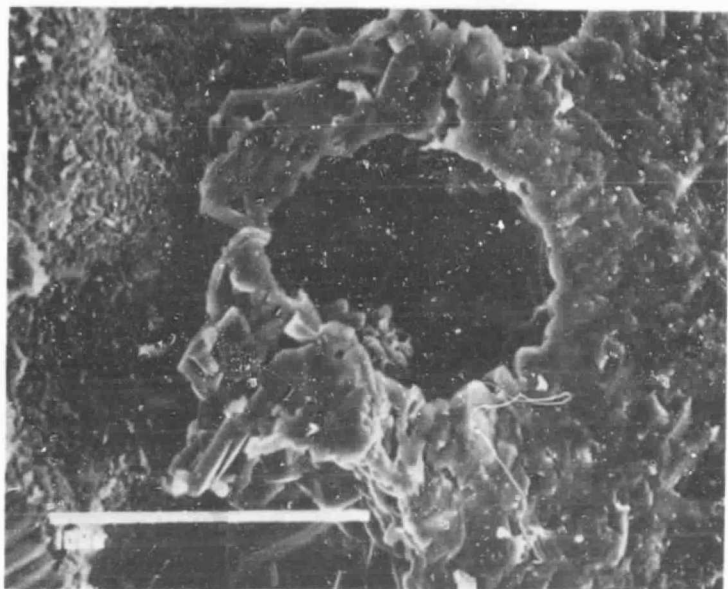
(a) As exposed to surface in green isopressed SiC.



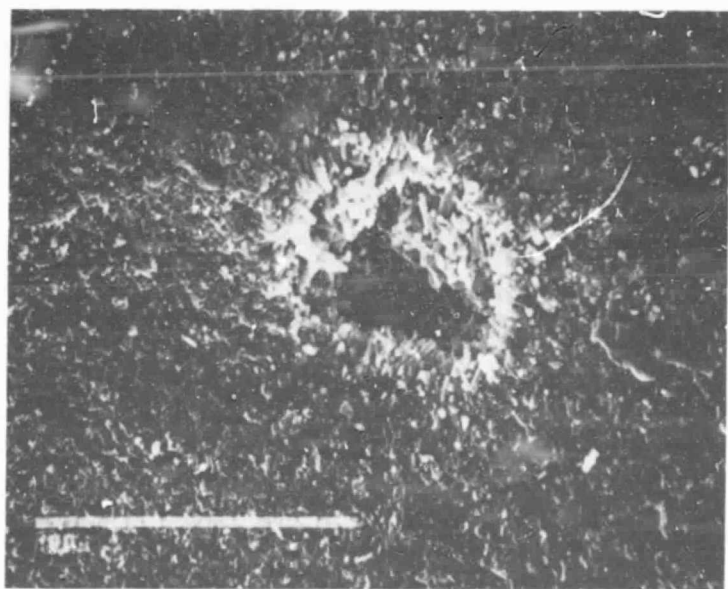
(b) As exposed to surface in green isopressed Si_3N_4 .

Figure 2. - Scanning electron micrographs of internal voids in SiC and Si_3N_4 bars.

ORIGINAL PAGE IS
OF POOR QUALITY



(c) On the fractured surface of sintered SiC.



(d) On the fractured surface of sintered Si₃N₄.

Figure 2. - Concluded.

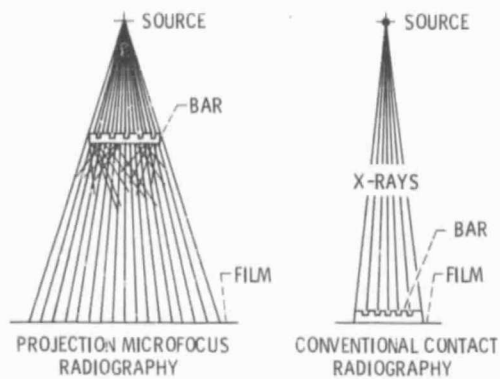


Figure 3. - The radiographic techniques used.

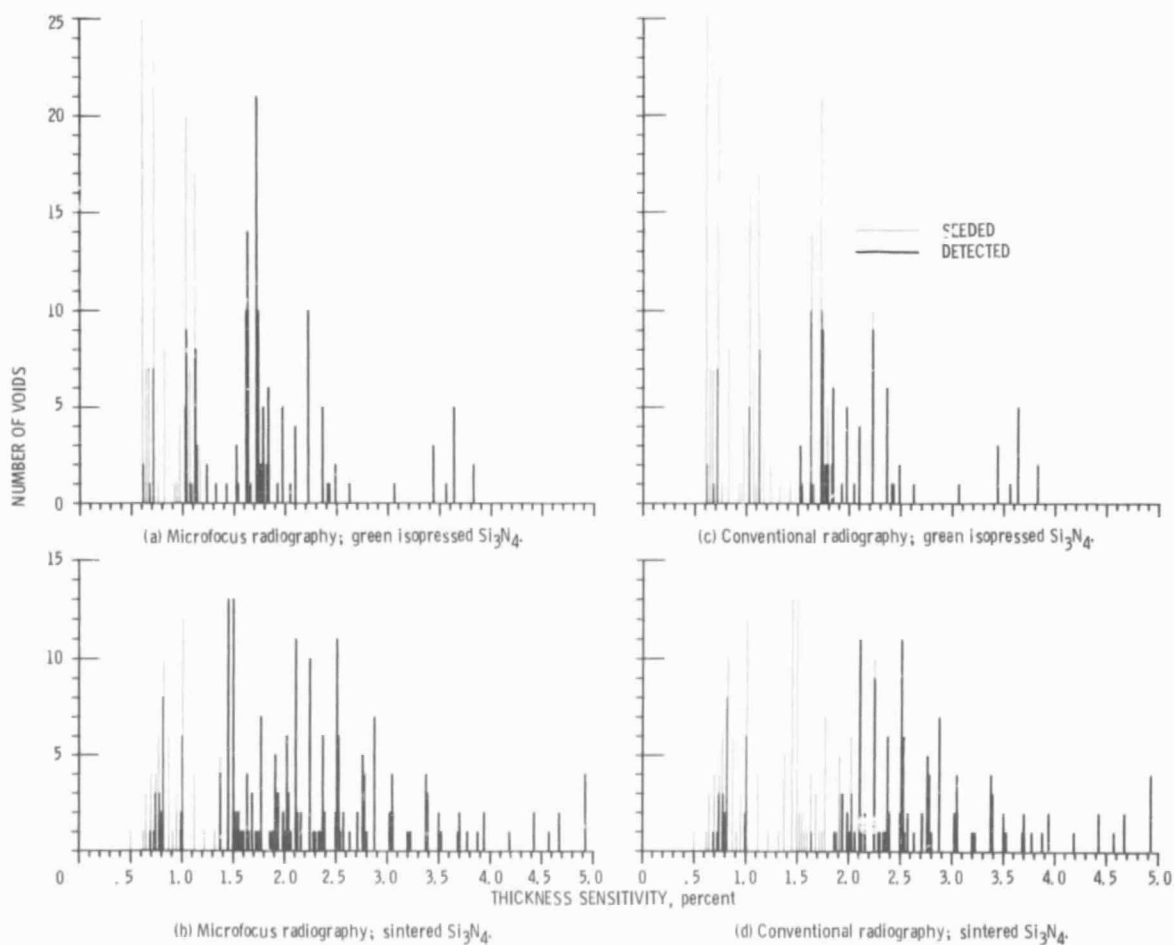


Figure 4. - Distribution of surface voids (seeded and detected) in Si_3N_4 bars calculated at 95 percent confidence level. Thickness sensitivity = (void dimension in x-ray beam direction)/(thickness of specimen in same direction).

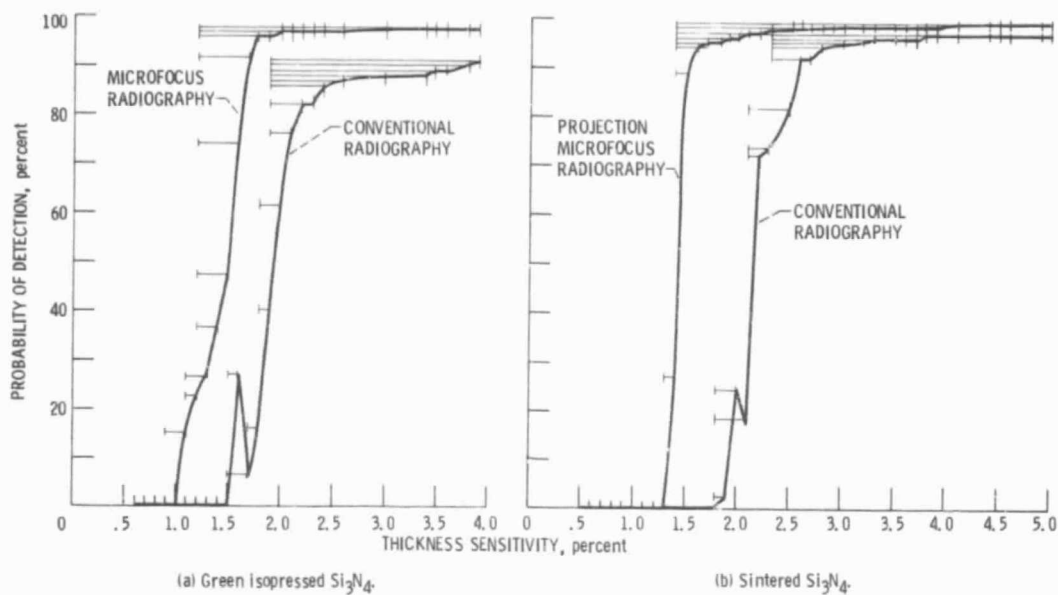


Figure 5. - Lower bound probability of detection of surface voids in Si_3N_4 bars calculated at 95 percent confidence level. Thickness sensitivity = (void dimension in x-ray beam direction)/(thickness of specimen in same direction).

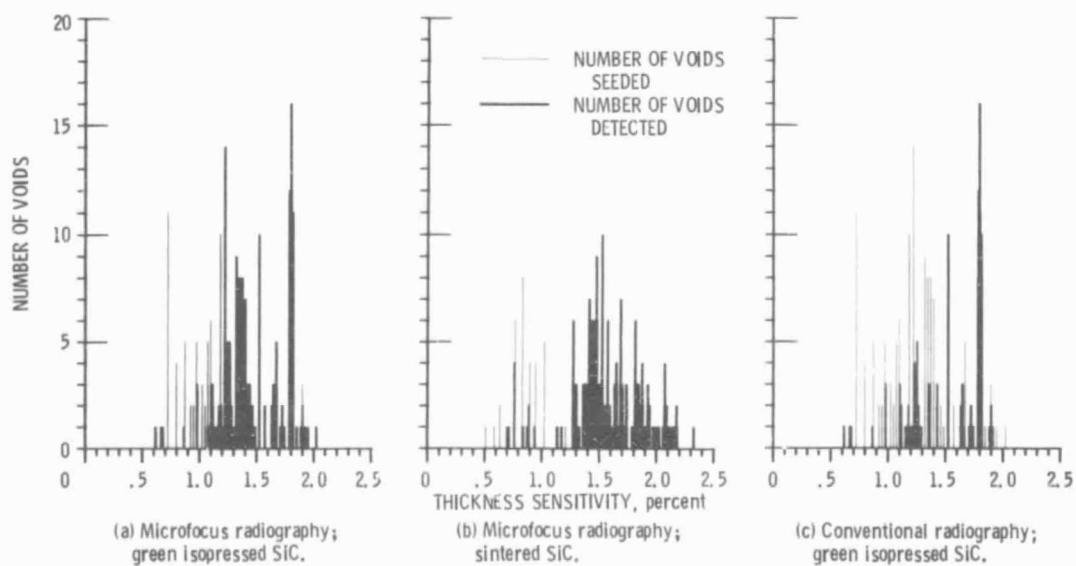


Figure 6. - Distribution of surface voids (seeded and detected) in SiC bars. Thickness sensitivity = (void dimension in x-ray beam direction)/(thickness of specimen in same direction).

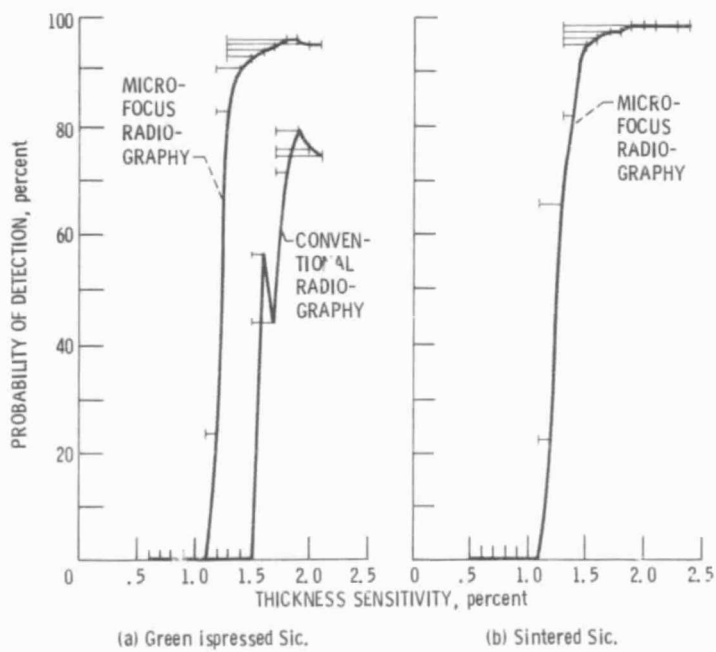
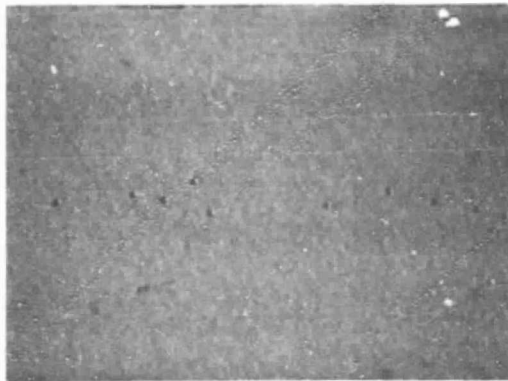


Figure 7. - Lower bound probability of detection of surface voids in Sic bars calculated at 95 percent confidence level. Thickness sensitivity = (void dimension in x-ray beam direction)/thickness of specimen in same direction.

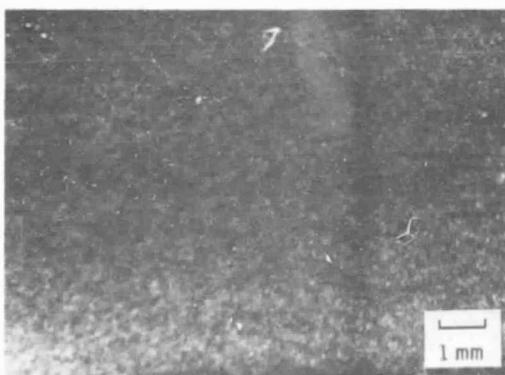
ORIGINAL PAGE IS
OF POOR QUALITY



(a) Optical photograph showing surface voids (dark spots).



(b) Microfocus radiograph of same region. Arrow: point to seeded voids.



(c) Conventional radiograph of same region.

Figure 8. - Sintered SiC bar with seeded surface voids as a result of decomposition of the $115\ \mu\text{m}$ spheres.